NOAA Technical Memorandum ERL WPL-121

COMPUTER DEMODULATION -- A NEW TECHNIQUE FOR COMPARISON RECEIVERS

C. L. Zhao
J. B. Snider
D. C. Hogg

Wave Propagation Laboratory
Boulder, Colorado
March 1985

noaa NATIONAL OCEANIC AND ATMOSPHERIC ADMINISTRATION / Environmental Research Laboratories

NOAA Technical Memorandum ERL WPL-121

COMPUTER DEMODULATION -- A NEW TECHNIQUE FOR COMPARISON RECEIVERS

C. L. Zhao
J. B. Snider
D. C. Hogg

Wave Propagation Laboratory
Boulder, Colorado
March 1985

UNITED STATES
DEPARTMENT OF COMMERCE

Malcolm Baldrige,
Secretary

NATIONAL OCEANIC AND
ATMOSPHERIC ADMINISTRATION

Environmental Research
Laboratories

Vernon E. Derr,
Director

NOTICE

Mention of a commercial company or product does not constitute an endorsement by NOAA Environmental Research Laboratories. Use for publicity or advertising purposes of information from this publication concerning proprietary products or the tests of such products is not authorized.

CONTENTS

COMPUTER DEMODULATION -- A NEW TECHNIQUE FOR COMPARISON RECEIVERS

C. L. Zhao, J. B. Snider, and D. C. Hogg

NOAA/ERL/Wave Propagation Laboratory

Boulder, Colorado 80303

ABSTRACT

We describe a new processing technique for use with comparison receivers whereby demodulation of the switched input signal is accomplished in computer software rather than in receiver hardware. Results obtained when the method is applied to an existing dual-channel microwave radiometer are presented.

1. BACKGROUND

A microwave radiometer is essentially a noise receiver. The noise power available at the terminals of a lossless antenna is given by $P = k T_a B$, where k is Boltzmann's constant, T_a is the antenna temperature, and B is the bandwidth of the predetection amplifier. A typical radiometer receiver is capable of detecting changes in T_a of the order of 1 K or less. If a receiver bandwidth B = 1 MHz, this corresponds to a change in power of $\Delta P \cong 1.3 \times 10^{-17}$ W, which is several orders of magnitude smaller than the internal noise power of the receiver itself. It is very difficult to get such a high degree of measurement precision by using the normal, total power receiver. In 1946 R. H. Dicke designed a new type of receiver, which successfully detected changes of the order of 1 K (Dicke, 1946).

The principle of the Dicke radiometer is to compare the input signal level with a reference signal level for measurements of the input power.

Operationally, this procedure can be realized by modulating the receiver input and synchronously demodulating the output (see Fig. 1). The function of the synchronous demodulator is to change the polarity of the detected voltage in synchronism with the position of the input switch. When this is properly done the final output of the integrator is proportional to the difference between the detected voltage due to the energy received from the antenna and the detected voltage due to the energy received from the reference. Since each of these detected voltages contains the same receiver noise component, the action of the demodulator removes this component from the final d.c. output.

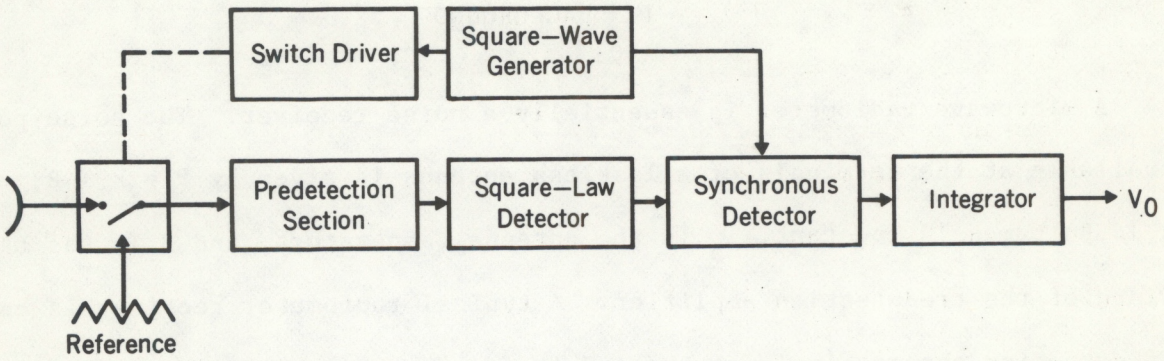

Figure 1. Conventional Dicke switched radiometer.

The design of the WPL dual-channel radiometer extends the normal Dicke design by adding a second calibration source, the "hot load", to the switching sequence (Hogg et al., 1983). The block diagram of the electronics is shown in Fig. 2. Two synchronous detectors are used for each frequency channel to

produce a continuous self-calibration of the radiometer. One synchronous detector is gated to detect the power difference between the antenna and reference load; the other is gated to detect the difference between the reference and the hot load. The voltage produced by the second synchronous detector is in effect a monitor of any changes in gain and is used as an automatic-gain-control (AGC) level that is applied in the computer. The output from the first synchronous detector is referred to as the data channel. The synchronous oscillators control the switching sequence of the ferrite switch and the gating of the synchronous detectors.

As described above the dual-channel radiometer uses separate hardware units for data and AGC synchronous detector circuitry, respectively. A disadvantage of this situation is that if the gain of either or both synchronous detectors changes, a false AGC information will be sent to the computer to correct the data channel, and therefore cause an error in the data.

To eliminate errors due to synchronous detector gain changes, we have conducted a preliminary study of a revised method of synchronous detection. In the new scheme, demodulation takes place in the computer software rather than in hardware. The new system block diagram is shown in Fig. 3. Hardware and software design considerations and experimental results are discussed in the following sections.

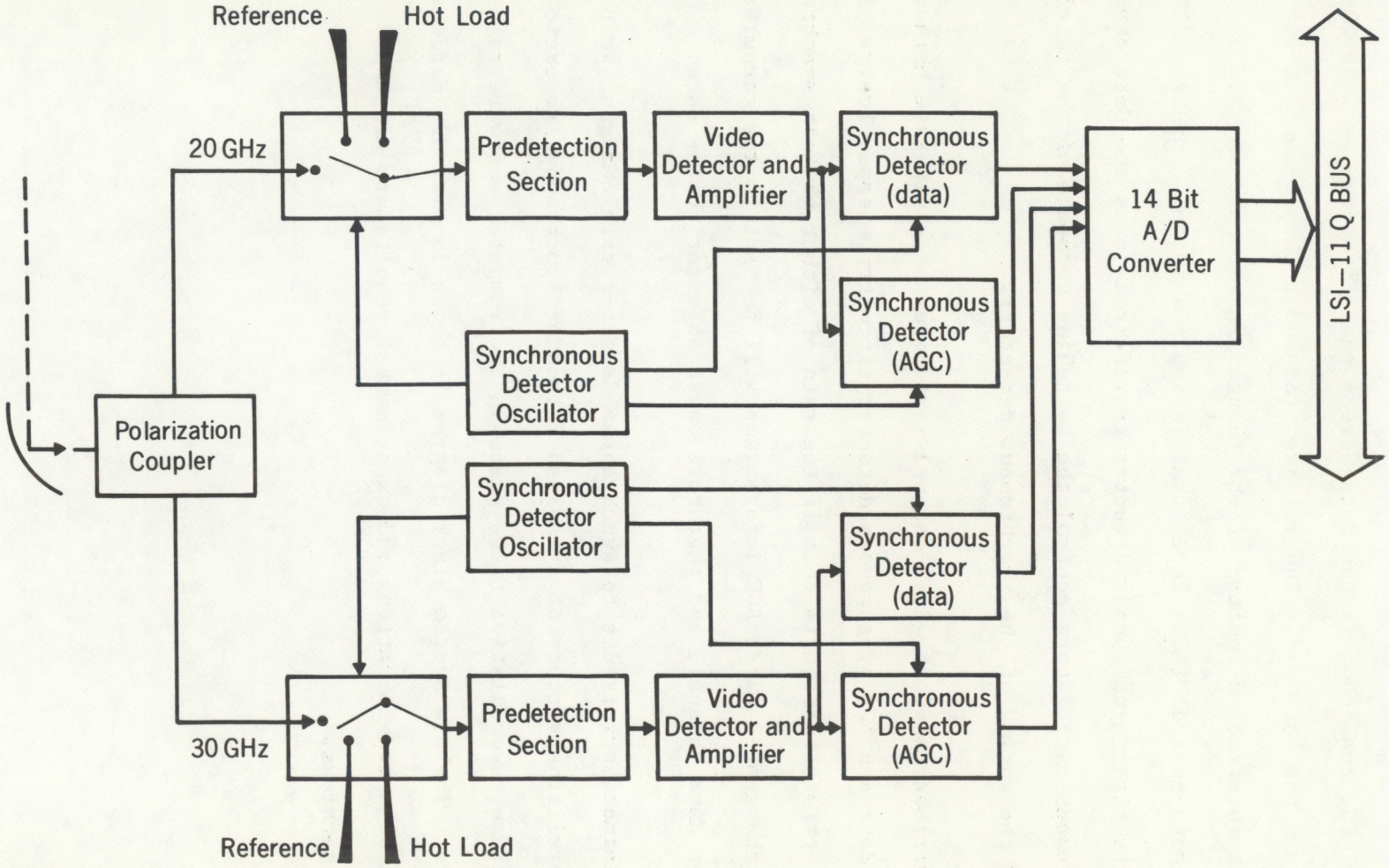

Figure 2. Dual-channel radiometer schematic using synchronous detection by hardware.

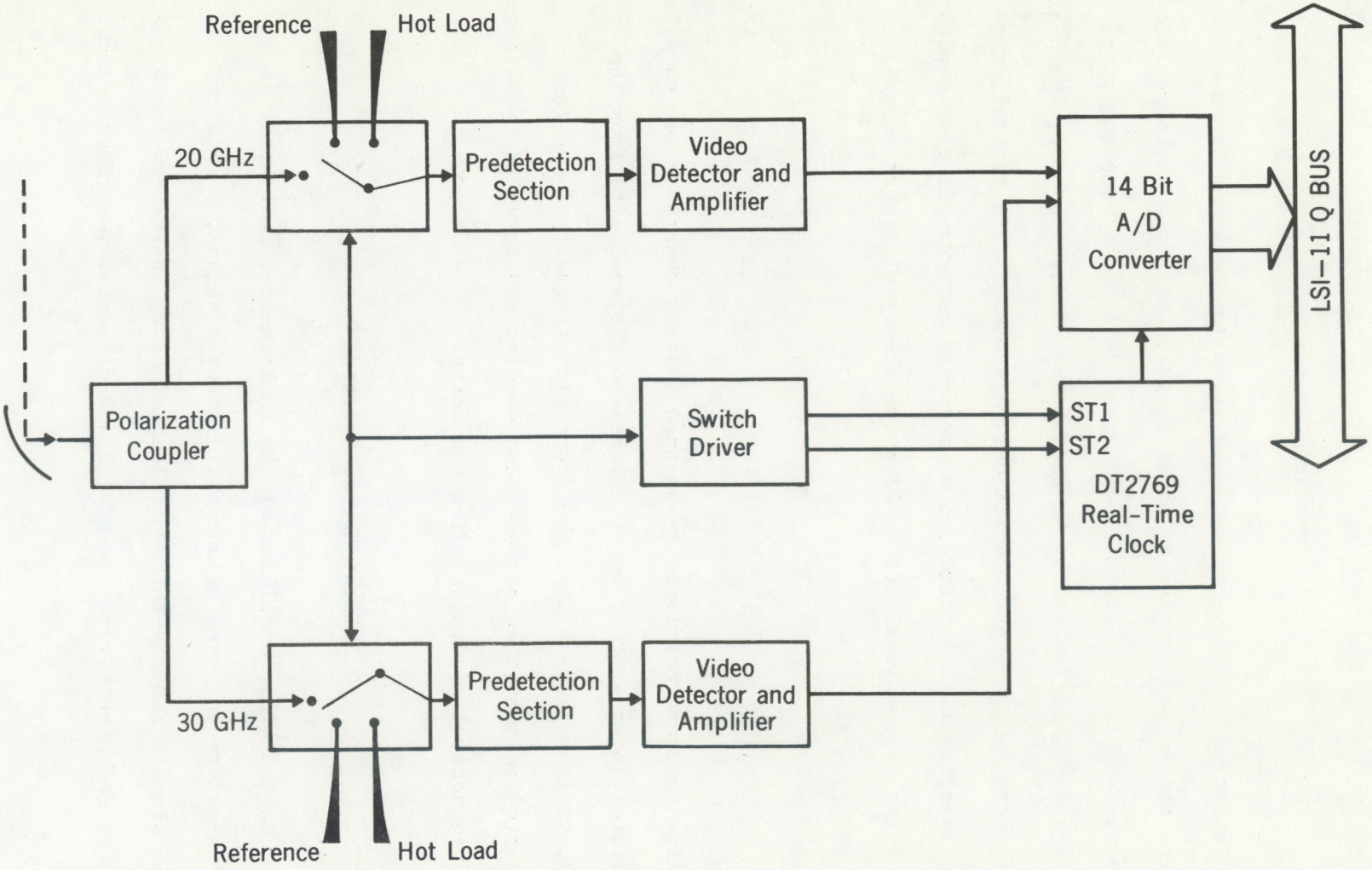

Figure 3. Dual-channel radiometer schematic using synchronous detection by computer.

2. SAMPLING RATE CONSIDERATION

2.1 Sampling Theorem

Sampling is periodic sensing or periodic measuring of a continuous signal quantity, where the measuring time is small compared with the periodic interval. Therefore, some of the information is lost during the sampling process. It is the purpose of sampling theory to define the conditions under which all the information can be, at least theoretically recovered. In general, the output of the sampling switch f*(t) can be regarded as a sampling wave p(t) modulated with the input signal f(t). From the theory of linear superposition, it is given by

$$f^*(t) = f(t)p(t) \ . \tag{2.1}$$

The sampling theorem, developed by Shannon (1948), describes how to select the sampling rate: In order to recover a continuous signal f(t) from the sampled f*(t), it is necessary that the repetition frequency f_r of the sampling wave p(t) be such that at least two samples are taken of the highest significant frequency of f(t), including the noise.

2.2 Input Signal Spectrum

The output of the video amplifier of the dual-channel radiometer is a three-stepped waveform composed of one-third antenna signal, one-third reference load signal, and one-third hot load signal. In the new technique, this waveform is fed directly to the DT2782 A/D converter for the sampling

process. This input signal f(t) to the A/D converter can be considered as follows:

$$f(t) = \begin{cases} 0 & (0 < t < T/3) \\ R & (T/3 < t < 2T/3) \\ H & (2T/3 < t < T) \end{cases} \tag{2.2}$$

where T is the period of the three-junction switchable circulator; R and H are constants.

To determine the highest significant frequency of f(t), it is expanded in terms of the Fourier series. The half-range expansions of f(t) are

$$f(t) = A_o + \sum_{n=1}^{\infty} A_n \cos \frac{n\pi}{T} t \tag{2.3}$$

where

$$A_o = \frac{1}{T} \int_o^T f(t)dt = \frac{R+H}{3}$$

$$A_n = \frac{2}{T} \int_o^T f(t) \cos \frac{n\pi t}{T} dt$$

$$= \frac{4}{n\pi} \left(R \cos \frac{n\pi}{2} \sin \frac{n\pi}{6}\right) + \frac{2H}{n\pi} \left(\sin n\pi - \sin \frac{2n\pi}{3}\right) .$$

Numerical evaluation of the Fourier coefficients shows that A_n converges very slowly for $n > 31$. Hence higher order harmonics contribute little to recovery of f(t).

The highest significant frequency is more obvious if we calculate the partial sums of the Fourier expansions (Eq. 2.3), which are given by

$$S_i = A_o + \sum_{n=1}^{i} A_n \cos \frac{n\pi}{T} t \ .$$

Figure 4 indicates that the series is convergent and has the sum f(t) for n = 31. Therefore the 31st order harmonic of the signal frequency f_s can be considered as the highest significant frequency of the input signal f(t). From the sampling theorem, the sampling rate f_r should be at least equal to two times the highest significant frequency of f(t), that is,

$$f_r > 2 \times 31 \times f_s \tag{2.4}$$

where $f_s = \frac{1}{T}$, and T is the switching period of the three-junction switchable circulator.

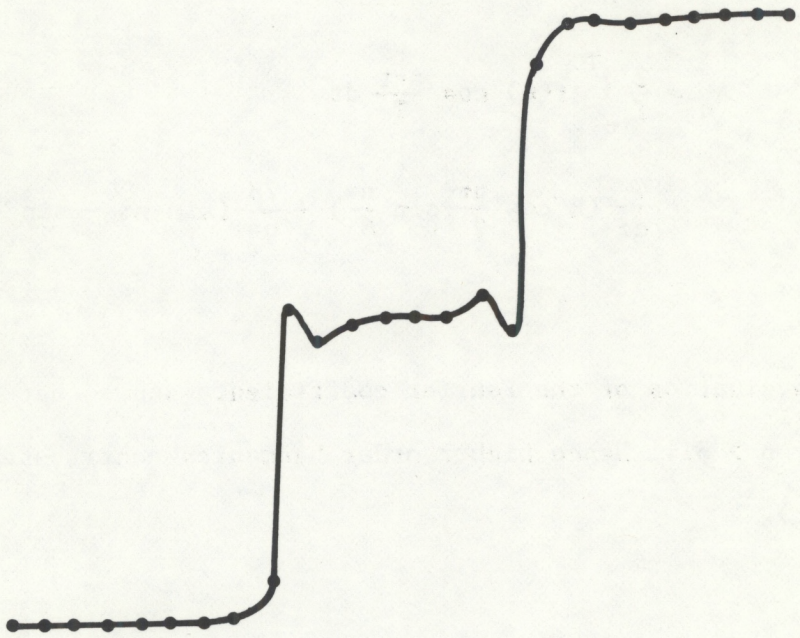

Figure 4. Waveform recovery using 31 terms of Fourier series expansion.

Another thing to be considered is the noise. We know the radiometer is essentially a noise receiver. Therefore, the input signal consists of the white noise, which can be any frequency. If there is no other filter in the signal path, the highest noise frequency is determined by the video amplifier bandwidth. Clearly to prevent excess contamination of the signal by receiver noise, the video amplifier bandwidth, f_v should be limited to

$$f_v = \frac{f_r}{2} . \tag{2.5}$$

3. SYNCHRONOUS DETECTION DESIGN

3.1 Procedure

In the revised system, the three stairstep output of the video amplifier is sent to an A/D converter instead of to the two synchronous detectors. In order to perform synchronous detection in the software, the signal from the video amplifier must be processed in a special manner. It is necessary to average the samples for each step (reference, hot load, and antenna), then take the difference between the antenna signal and reference load as the DATA signal, and the difference between reference and hot load as the AGC signal. The computer collects the samples, puts them serially into a data buffer, and then sorts the data according to the modulating sequence. After these processing steps, the data arrays are ready for the mathematical algorithms that calculate the amount of vapor and liquid.

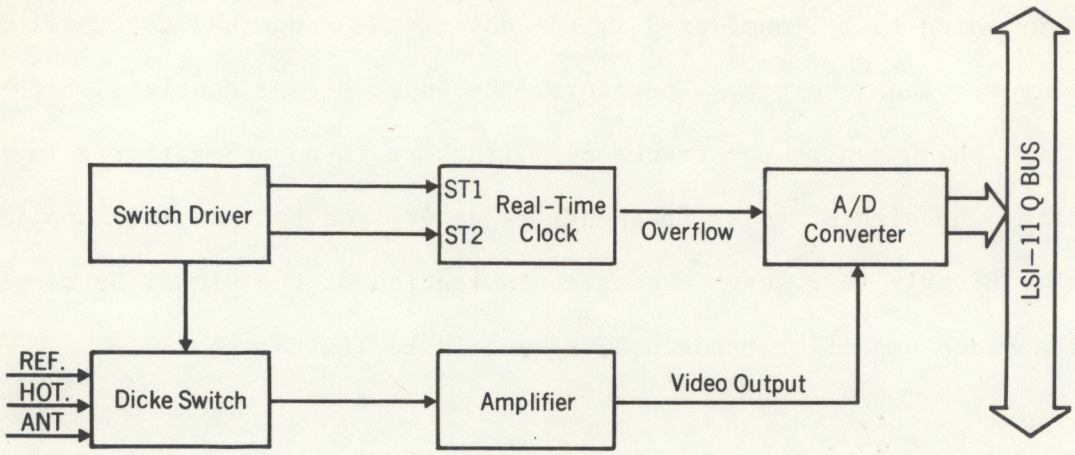

Figure 5. Data acquisition scheme. The signals from the switch driver are used to fire the two Schmitt triggers of the Real-Time Clock (RTC). Schmitt trigger 1 is to generate a time base for the clock counter. Schmitt trigger 2 is used to turn the clock on.

3.2 Hardware Description

The data acquisition scheme is shown in Fig. 5. The heart of the new system is the switch driver and sample control card. This single hardware module has two main functions: to drive the switchable circulator, and to produce the sample pulses. The circuits (Fig. 6) that generate the waveforms for switching and sampling are controlled by a 2048 bit programmable read only memory (PROM). The PROM contains four programs (see Appendix), one for normal operation and three for various calibration modes. Mode selection is performed by the computer software which addresses two input lines of the PROM that serve as program selector. Calibration consists of periodically switching the radiometer antenna inputs to the reference and calibration terminations at specified intervals. The calibration programs cause the radiometers to sample the known noise signals from the temperature-controlled terminations, providing a measurement of system sensitivity.

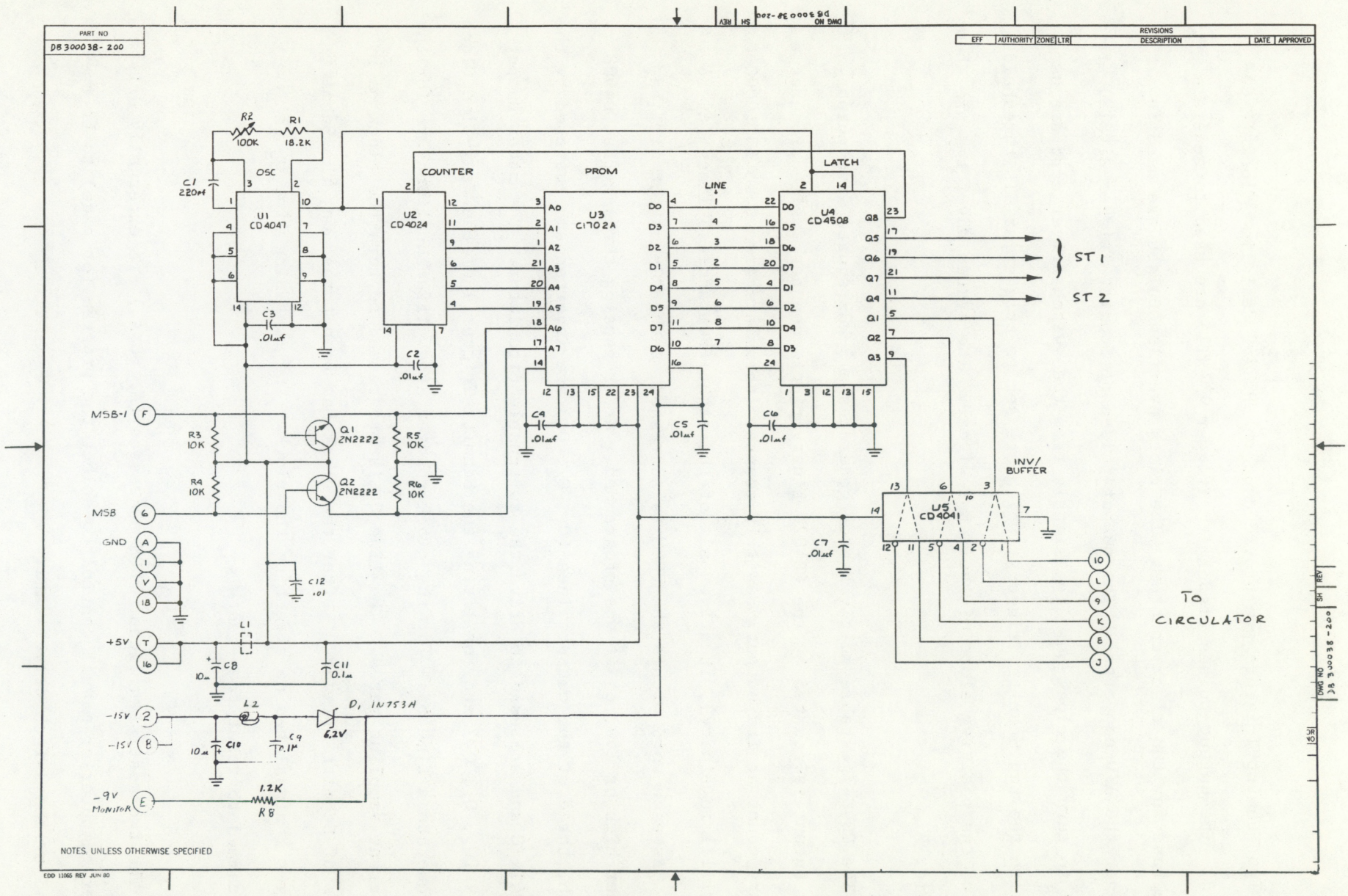

Figure 6. Switchable circulator/synchronous sampling driver unit.

Two Schmitt Triggers are provided on the DT2769 Real-Time Clock (RTC) board. The output pulses of Schmitt Trigger 1 (ST1) are used to generate a time base for the clock counter. The clock overflow pulses are used to trigger the A/D converter. The output pulses of Schmitt Trigger 2 (ST2) are used to turn the clock on. The signals from the switch driver card are used to fire the two Schmitt Triggers, which are set to trigger at TTL thresholds and on the positive slope of the input signal. The system waveforms are shown in Fig. 7.

The CD4047 astable multivibrator generates a 3-kHz square wave output. This output is counted by the CD4024 binary ripple counter, which produces a binary count at its output. As this counter increments from 0 to 63 (000000 to 111111 in binary), it drives six of the eight PROM address lines (A_0 to A_5). As each word within the PROM is addressed, each PROM output will be either high or low, as it was programmed. After passing through the CD4508 latch, three of the output lines (Q_1, Q_2, Q_3) are inverted and buffered by the CD4041 IC and are used to drive the switchable circulator. The other output lines (Q_5, Q_6, Q_7) are for firing the Schmitt Trigger 1 of the Real-Time Clock to generate a time base for the clock counter; the different lines are for the different sampling rates. The line Q_4 is programmed to turn the clock on by means of Schmitt Trigger 2; after the clock has been turned on, the Schmitt Trigger 2 signal has no effect on the clock. The remaining line Q_8 is programmed to reset the counter.

The two most significant PROM addresses (A_6 to A_7) are externally driven under computer or manual control to select the program (or page) to be executed by the switch driver card.

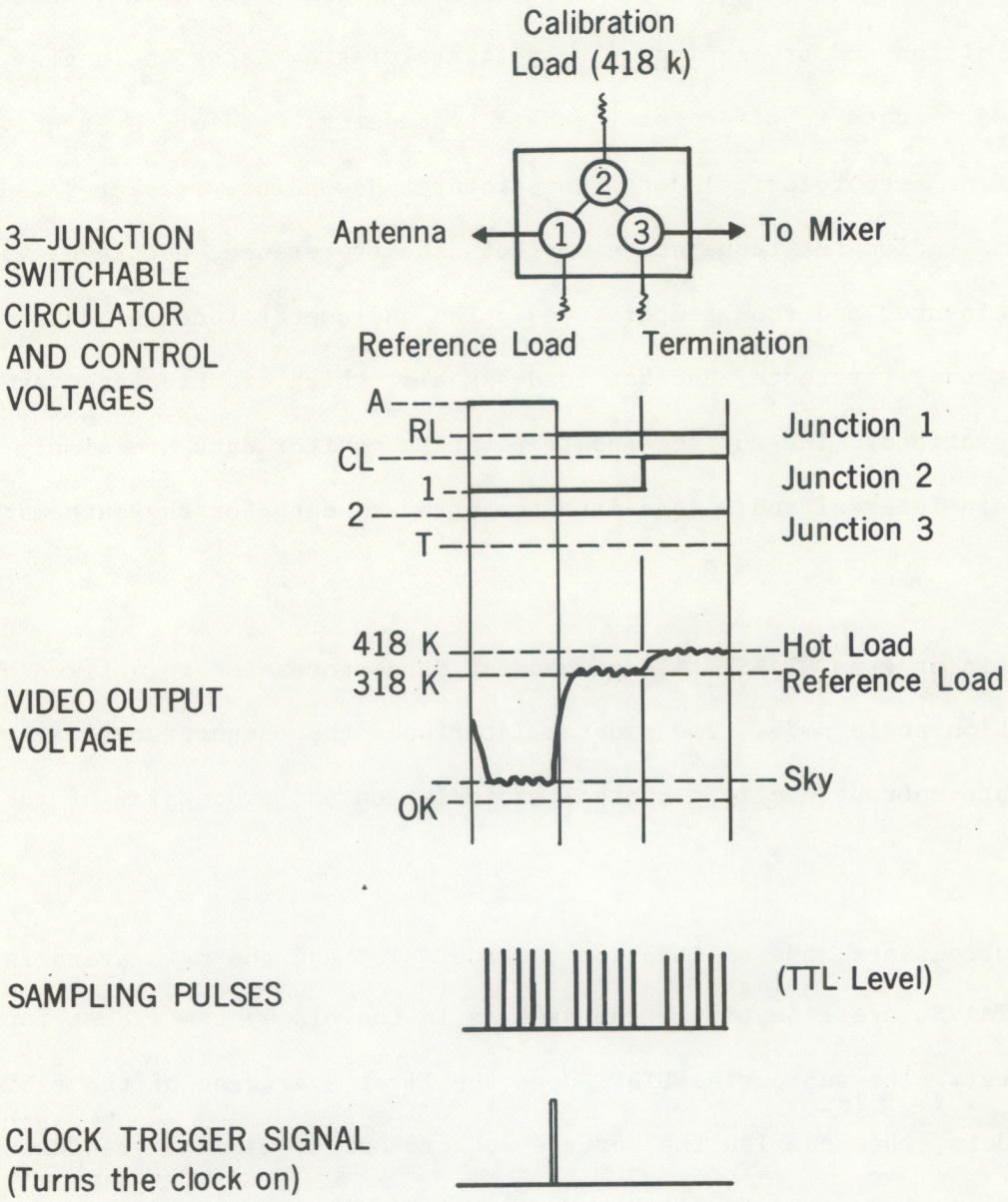

Figure 7. System waveforms.

3.3 Software Description

This section describes the actual computer program and subroutines for data acquisition and processing. The software diagram is shown in Fig. 8. Three types of data required for the data processing: radiometer receiver data, surface meteorological data (temperature, dew-point, pressure, and rain gauge), and radiometer temperature monitor data (reference, hot load, waveguide, enclosure, and room temperature). The radiometer receiver data consist of the antenna, reference, and hot load signals, which are processed as previously described. The surface and temperature monitor data are simply taken at a certain interval and placed into the array of data for the mathematical processing.

The main program DTATST is designed for data processing in a fixed azimuth and elevation angle mode. The program interfaces the computer hardware with the software subroutines that control manipulation and processing of the input data.

Two subroutines, the calibration routine AUTOC and the main averaging routine DTAAVE, are essentially the same as in the old system except for the time counter. The subroutine DTAPT does the first averaging of the radiometer receiver data, then samples the surface meteorological data and radiometer temperature monitors and finally sorts them out into a meaningful array.

The subroutine DTAPOT, called from the routine DTAPT, initiates and controls real-time sampling of the analog input channel. It takes the data as first read in and later processes them in another routine called DISPLA, which uses the DATA TRANSLATION (DTLIB) software routines SETR and RTS to do real-time sampling. The subroutine DISPLA sorts sequential data into temporary

arrays sorted according to the modulating sequence. Finally the difference between the antenna and reference signals as the atmospheric data, and the difference between the reference and hot load signals as the AGC data, are taken and inserted into the final data array for the conventional processing procedure that calculates amounts of water vapor and liquid.

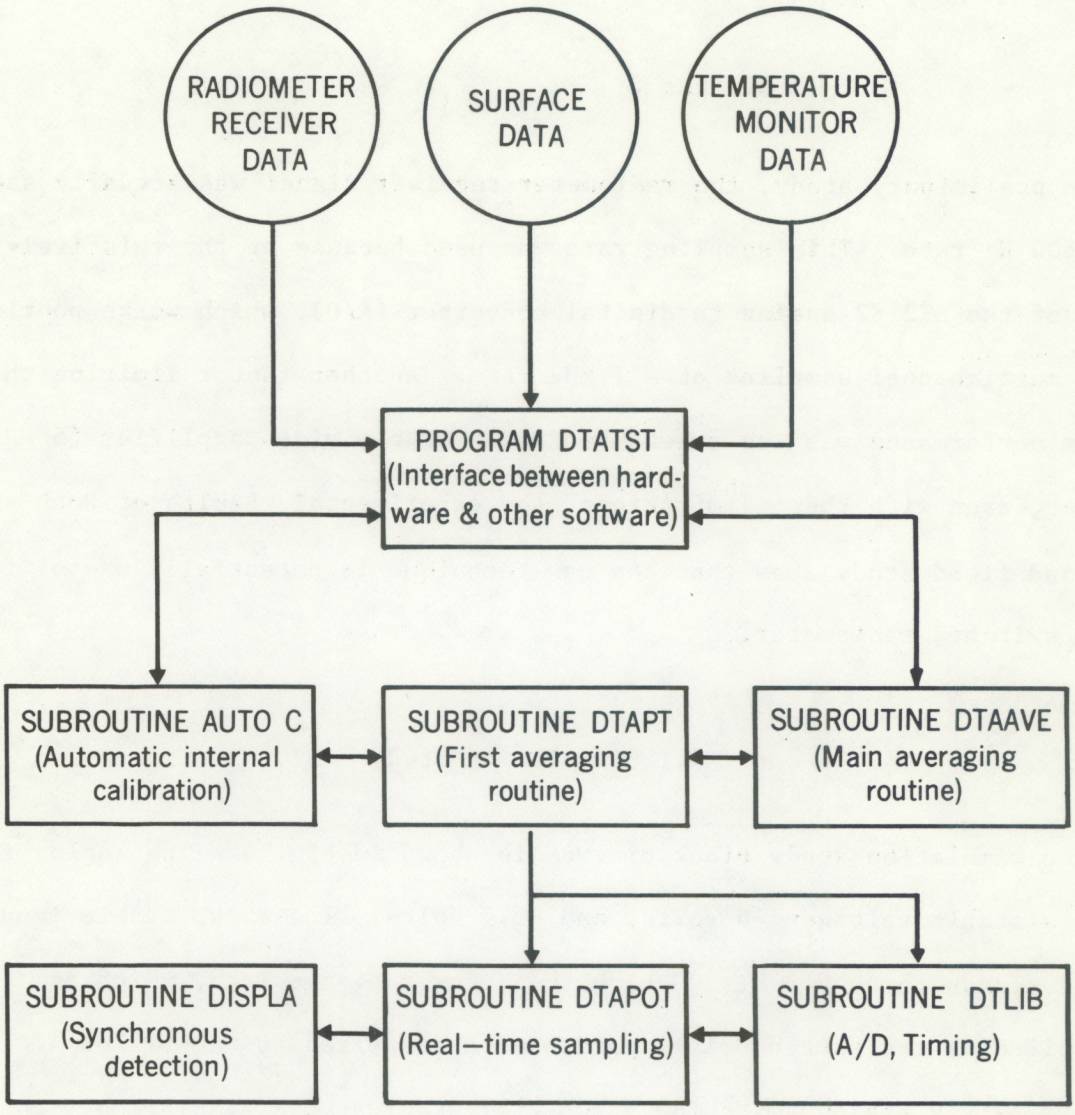

Figure 8. Data processing software.

4. EXPERIMENTAL RESULTS

The sampling system used in the preliminary evaluation of the computer demodulation technique was designed to retain compatibility with the present processor and radiometer electronics. As a result, the equipment was operated in less than an optimum configuration.

For example, from (2.4) for $f_s = 50$ Hz, we have

$$f_r > 3.1 \text{ kHz} . \tag{4.1}$$

In the preliminary study, the radiometer receiver signal was actually sampled at a 600 Hz rate. This sampling rate was used because of the relatively slow speed of the DT2782 analog to digital converter (A/D), which works poorly using multichannel sampling at a 1 kHz rate. Another factor limiting the system performance was the excess bandwidth of the video amplifier (5 kHz). However, even with these limitations, the experimental results of both simulation and field study show that the new technique is potentially useful for the Dicke switched radiometer.

4.1 Simulation Study

The simulation study block diagram is shown in Fig. 9. The analog inputs are two stable voltages: 6 volts, and ~5.4 volts. These two stable input voltages pass through a HI-200 high frequency analog switch, which is controlled by the switch driver card, and are applied to the DT2782 A/D converter. After analog switching a two-stairstep, stable simulation signal is obtained for real-time sampling. The computer software processes the sampled

data and takes the difference between the input voltages. An example of computer output during the simulation is shown in Fig. 10. Each line corresponds to a 5-s sample average. The results show that the processor is very stable and reliable.

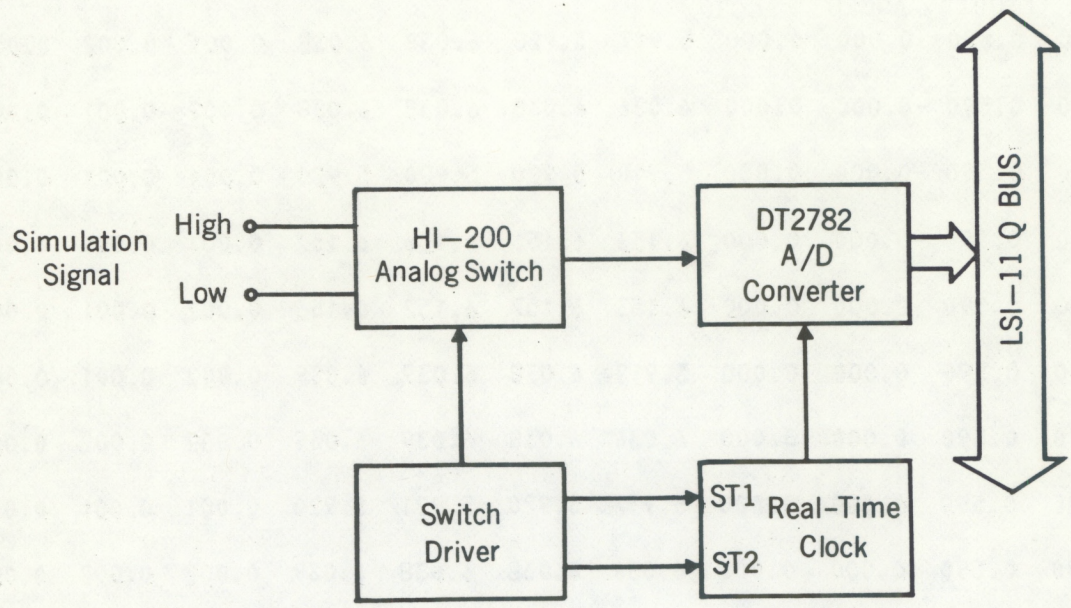

Figure 9. Configuration for simulation study.

```
.RUN DTATST
DUAL CHANNEL RADIOMETER DATA PROCESSING TEST PROGRAM
  0.590   0.590   0.000   0.000   5.917   5.920   5.920   5.920   0.001   0.001   0.001

  0.590   0.590   0.000  -0.000   6.036   6.038   6.133   6.157   0.001   0.001   0.001

   0.590    0.590    0.000   -0.000   59.765   59.792  160.267  160.384
   0.014    0.014    0.015    0.015    0.015    0.015    0.016    0.000     2
 VAPOR  LIQUID  AGC20    AGC30
  0.590   0.590  -0.000   0.000   5.917   5.920   6.038   6.038   0.001   0.002   0.001

  0.590   0.590  -0.000   0.000   6.036   6.038   6.038   6.038   0.002   0.001   0.001

  0.590   0.590  -0.000   0.000   5.918   5.920   5.920   5.920   0.001   0.001   0.001

  0.590   0.590  -0.000   0.000   6.153   6.156   6.156   6.157   0.001   0.001   0.001

  0.590   0.590  -0.000   0.000   6.153   6.157   6.157   6.156   0.002   0.001   0.002

  0.590   0.590   0.000   0.000   5.918   6.038   6.039   6.039   0.002   0.001   0.001

  0.590   0.590   0.000   0.000   6.036   6.038   6.039   6.039   0.002   0.002   0.002

  0.590   0.590   0.000  -0.000   5.917   5.920   5.921   5.920   0.001   0.001   0.001

  0.590   0.590   0.000   0.000   6.036   6.038   6.038   6.039   0.002   0.002   0.002

  0.590   0.590  -0.000  -0.000   6.154   6.156   6.157   6.156   0.001   0.001   0.001

  0.590   0.590  -0.000  -0.000   5.918   6.038   6.038   6.038   0.002   0.001   0.001

  0.590   0.590   0.000   0.000   6.035   6.038   6.038   6.039   0.001   0.001   0.001

  0.590   0.590   0.000   0.000   5.917   5.920   5.921   5.920   0.002   0.002   0.002
```

Figure 10. An example of computer simulated video sampling (six samples for each step, sampling rate of 600 Hz). The simulation signal is a two stairstep stable voltage. The first two columns show the data channels, the second two show the AGC channels; the AGC equals zero because the reference simulation signal is the same as the hot load signal.

4.2 Field Experiments

During the first three weeks of October 1984, we installed the new system in the WPL dual-channel radiometer for a field experiment at the Boulder Atmospheric Observatory (BAO). A simple system modification involved replacement of the post-detection hardware modules (four synchronous detector cards) and two oscillator cards with a new switch driver card. For convenience, jumpers were used to connect the video amplifier output to the analog input of the A/D converter (see Figs. 2 and 3).

The sampling period and integration times are set in a computer "constants" file to allow simple revision to obtain a desired sensitivity. This is another advantage of performing demodulation in the software. Theoretical and experimental system sensitivity vs. integration time are shown in Fig. 11.

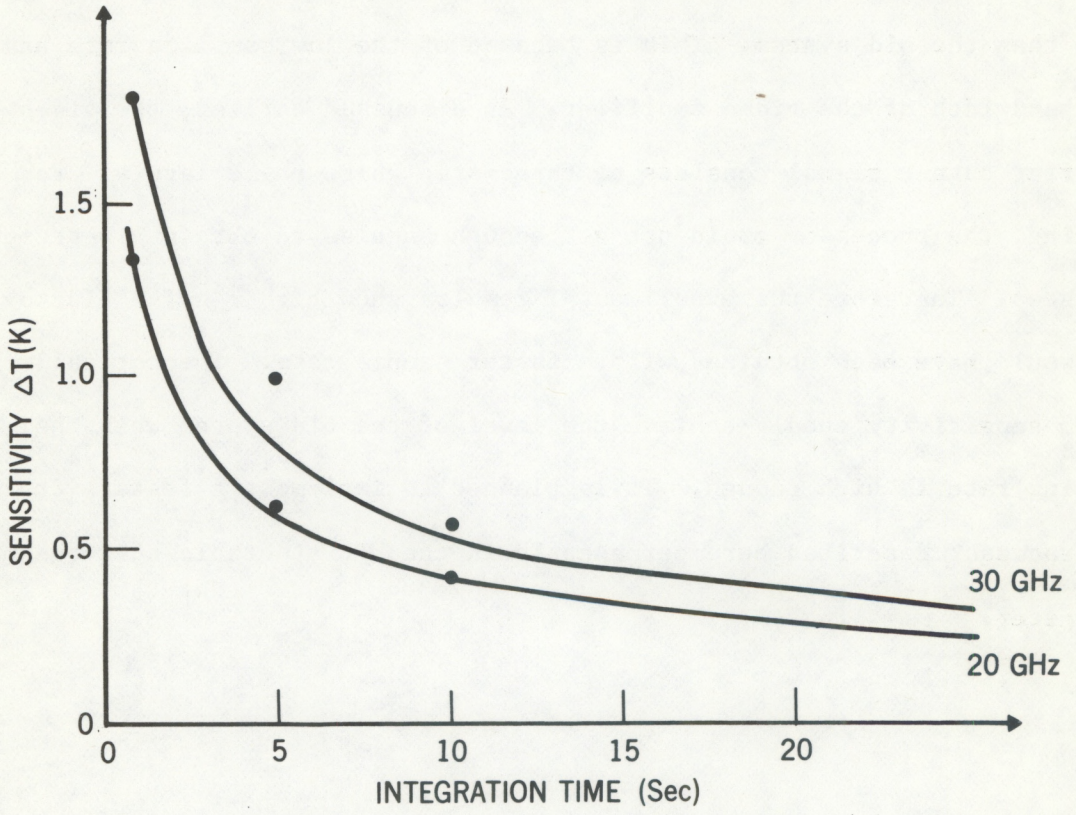

Figure 11. Radiometer sensitivity versus integration time. Solid lines are theoretical values; the points show experimental results.

In the field experiments, a 16-channel 14-bit A/D converter is used to sample the video amplifier output, the temperature of the reference and calibration sources, the temperature of the waveguide and the radiometer enclosure, and the outside surface data. The A/D converter samples at a rate of 600 Hz; these data are averaged for 10 seconds before being reduced to precipitable water vapor and liquid water by the retrieval algorithms. The unreduced 10-s data are further averaged over 5-min periods before being recorded on the computer's disk. Periodically, the 5-min averaged precipitable water vapor and integrated liquid data are displayed in a simple symbol plot (Fig. 12). Performance of the system during the field experiment is summarized in Table 1.

In the experiment we found the new system to be very flexible and reliable. However, Table 1 shows that the new system did have a higher noise level than the old system. This is because of the low sampling rate and the wide bandwidth of the video amplifier. As discussed earlier, the video amplifier output signal consists of three-step white noise levels. For slow sampling, the processor could not get enough samples to obtain a best mean for each step. Therefore the experimental results show higher noise fluctuations than would have been obtained with a faster sample rate. Theoretically the system sensitivity should achieve the level of the old system when the sampling rate is high enough. It is planned to implement a faster version of the processor described here permanently in the WPL steerable dual-channel radiometer.

```
                                    0         1         2         3         4         5
DAY TIME  ELEV  AZIM  VAP  LIQ  123456789 123456789 123456789 123456789 123456789
    GMT   DEG   DEG   CM   MM                V(CM)               L(MM)

279 2120  90.0  0.1   1.3 -0.1 L           V
279 2125  90.0  0.1   1.4 -0.1 L            V
279 2130  90.0  0.1   1.3 -0.1 L           V
279 2135  90.0  0.2   1.3 -0.1 L           V
```

Figure 12. Teletype record at the BAO showing precipitable water vapor (V) and cloud liquid (L).

Table I. System Performance

	Vapor channel			Liquid channel		
Center frequency	20.6 GHz			31.65 GHz		
IF bandpass	50-550 MHz			50-550 MHz		
VA bandpass	0-5 kHz			0-5 kHz		
System noise	650 K			700 K		
Integration time	1 s	5 s	10 s	1 s	5 s	10 s
Average (AGC)	483 mv	483 mv	485 mv	475 mv	474 mv	474 mv
Standard deviation	6.5 mv	3.1 mv	2.1 mv	8.7 mv	5.1 mv	3.2 mv
Coefficient of variation (percent)	1.35	0.64	0.43	1.83	1.07	0.67
Sensitivity	1.3 K	0.6 K	0.4 K	1.8 K	1.1 K	0.6 K

5. SUMMARY

We have investigated the feasibility of using software rather than hardware to do phase detection in the dual-channel radiometer. The preliminary study has shown that the new technique of using computer sampling of the video output is practicable for the Dicke switched radiometer. The main advantages of the new sampling technique are as follows:

(1) Improved operation is achieved using the original system electronics but with fewer components.

(2) By using software to perform synchronous detection, the integration time can be easily varied. This feature is very useful in achieving different operational modes.

As described earlier, the preliminary study used a relatively low sampling rate because of hardware limitations. As a result, the noise level is higher than in the old system. The noise level can be reduced by increasing the sampling rate. However, this may require a larger memory and a faster processor. The noise level can also be improved by decreasing the bandwidth of the video amplifier. Both approaches will be implemented and studied.

Although the video sampling technique was applied here in microwave radiometry, the method could be used in any instrument that employs comparison switching.

6. REFERENCES

Dicke, R. H., 1946: The measurement of thermal radiation at microwave frequencies, Rev. Sci. Instr., 17, 268-275.

Hogg, D. C., F. O. Guiraud, J. B. Snider, M. T. Decker, and E. R. Westwater, 1983: A steerable dual-channel microwave radiometer for measurement of water vapor and liquid in the troposphere. J. Appl. Meteorol. 22, 789-806.

Shannon, C., 1948: The philosophy of pulse code modulation. Proc. IRE, 36, 1328-1331.

Shannon, C., 1949: Communication in the presence of noise. Proc. IRE, 37, 10-21.

APPENDIX A - Programmable Read Only Memory (PROM) for Computer Demodulation

Page 1 - Normal Data

ADDRS HEX	ADDRS DEC	DATA 8765	DATA 4321	MSB 0	MSB-1 0	Program Display
0	0	0100	0000			40
1	1	0100	1000			48
2	2	0100	0110			46
3	3	0100	1010			4A
4	4	0100	0000			40
5	5	0100	1100			4C
6	6	0100	0010			42
7	7	0100	1010			4A
8	8	0100	0100			44
9	9	0100	1000			48
A	10	0100	0010			42
B	11	0100	1110			4E
C	12	0100	0000			40
D	13	0100	1000			48
E	14	0100	0110			46
F	15	0100	1010			4A
10	16	0100	0000			40
11	17	0100	1100			4C
12	18	0100	0010			42
13	19	0100	1010			4A
14	20	0110	0000			60
15	21	0110	1000			68
16	22	0110	0110			66
17	23	0110	1010			6A
18	24	0110	0000			60
19	25	0110	1100			6C
1A	26	0110	0010			62
1B	27	0110	1010			6A
1C	28	0110	0100			64
1D	29	0110	1000			68
1E	30	0110	0010			62
1F	31	0110	1110			6E
20	32	0110	0000			60
21	33	0110	1000			68
22	34	0110	0110			66
23	35	0110	1010			6A
24	36	0110	0000			60
25	37	0110	1100			6C
26	38	0110	0010			62
27	39	0110	1010			6A
28	40	0101	0000			50
29	41	0101	1000			58

2A	42	0101	0110	56
2B	43	0101	1010	5A
2C	44	0101	0000	50
2D	45	0101	1100	50
2E	46	0101	0010	52
2F	47	0101	1010	5A
30	48	0101	0100	54
31	49	0101	1000	58
32	50	0101	0010	52
33	51	0101	1110	5E
34	52	0101	0000	50
35	53	0101	1000	58
36	54	0101	0110	56
37	55	0101	1010	5A
38	56	0101	0000	50
39	57	0101	1100	50
3A	58	0101	0010	52
3B	59	0101	1010	5A
3C	60	1000	0000	80
3D	61	0000	0001	01
3E	62	0000	0000	00
3F	63	0000	0000	00

ADDRS HEX	ADDRS DEC	DATA 8765	DATA 4321	MSB 0	MSB-1 1	Program Display
40	64	0100	0000			40
41	65	0100	1000			48
42	66	0100	0110			46
43	67	0100	1010			4A
44	68	0100	0000			40
45	69	0100	1100			4C
46	70	0100	0010			42
47	71	0100	1010			4A
48	72	0100	0100			44
49	73	0100	1000			48
4A	74	0100	0010			42
4B	75	0100	1110			4E
4C	76	0100	0000			40
4D	77	0100	1000			48
4E	78	0100	0110			46
4F	79	0100	1010			4A
50	80	0100	0000			40
51	81	0100	1100			4C
52	82	0100	0010			42
53	83	0100	1010			4A
54	84	0100	0000			↓
55	85	0100	1000			↓
↓	↓	↓	↓			↓
66	102	0100	0000			↓
67	103	0100	1000			↓
68	104	0100	0000			↓
↓	↓	↓	↓			↓
7B	123	0100	0000			↓
7C	124	1000	0000			80
7D	125	0000	0001			01
7E	126	0000	0000			00
7F	127	0000	0000			00

ADDRS HEX	ADDRS DEC	DATA 8765	DATA 4321	MSB 1	MSB-1 0	Program Display
80	128	0100	0000			40
81	129	0100	1000			48
82	130	0100	0110			46
83	131	0100	1010			4A
84	132	0100	0000			40
85	133	0100	1100			4C
86	134	0100	0010			42
87	135	0100	1010			4A
88	136	0100	0100			44
89	137	0100	1000			48
8A	138	0100	0010			42
8B	139	0100	1110			4E
8C	140	0100	0000			40
8D	141	0100	1000			48
8E	142	0100	0110			46
8F	143	0100	1010			4A
90	144	0100	0000			40
91	145	0100	1100			4C
92	146	0100	0010			42
93	147	0100	1010			4A
94	148	0110	0000			60
95	149	0110	1000			68
96	150	0110	0110			66
97	151	0110	1010			6A
98	152	0110	0000			60
99	153	0110	1100			6C
9A	154	0110	0010			62
9B	155	0110	1010			6A
9C	156	0110	0100			64
9D	157	0110	1000			68
9E	158	0110	0010			62
9F	159	0110	1110			6E
A0	160	0110	0000			60
A1	161	0110	1000			68
A2	162	0110	0110			66
A3	163	0110	1010			6A
A4	164	0110	0000			60
A5	165	0110	1100			6C
A6	166	0110	0010			62
A7	167	0110	1010			6A
A8	168	0110	0000			↓
A8	↓	↓	↓			↓
BB	187	0110	0000			↓
BC	188	1000	0000			80
BD	189	0000	0001			01
BE	190	0000	0000			00
BF	191	0000	0000			00

Page 4 - Used to Align

ADDRS HEX	ADDRS DEC	DATA 8765	DATA 4321	MSB 1	MSB-1 1	Program Display
C0	192	0100	0000			40
C1	193	0100	1000			48
C2	194	0100	0110			46
C3	195	0100	1010			4A
C4	196	0100	0000			40
C5	197	0100	1100			4C
C6	198	0100	0010			42
C7	199	0100	1010			4A
C8	200	0100	0100			44
C9	201	0100	1000			48
CA	202	0100	0010			42
CB	203	0100	1110			4E
CC	294	0100	0000			40
CD	205	0100	1000			48
CE	206	0100	0110			46
CF	207	0100	1010			4A
D0	208	0100	0000			40
D1	209	0100	1100			4C
D2	210	0100	0010			42
D3	211	0100	1010			4A
D4	212	0100	0000			↓
↓	↓	↓	↓			↓
E7	231	0100	1010			↓
E8	232	0100	0000			↓
↓	↓	↓	↓			↓
FB	251	0100	1010			↓
FC	252	1000	0000			80
FD	253	0000	0001			01
FE	254	0000	0000			00
FF	255	0000	0000			00